1 **Technical Note: Three-dimensional transient groundwater flow**

2 **due to localized recharge with an arbitrary transient rate in**

3 **unconfined aquifers**

4

5 **Chia-Hao Chang[1], Ching-Sheng Huang[1], and Hund-Der Yeh[1,*]**

6

7

10

11 [1] Institute of Environmental Engineering, National Chiao Tung University, Hsinchu, Taiwan

12

13 *** Corresponding Author**

14 Address: Institute of Environmental Engineering, National Chiao Tung University, 1001

15 University Road, Hsinchu 300, Taiwan

16 E-mail address: hdyeh@mail.nctu.edu.tw; Tel: 886-3-5731910; Fax: 886-3-5725958

17 **Abstract**

18   Most previous solutions for groundwater flow induced by localized recharge assumed

19 either aquifer incompressibility or two-dimensional flow in the absence of the vertical flow.

20 This paper develops a new three-dimensional flow model for hydraulic head variation due to

21 localized recharge in a rectangular unconfined aquifer with four boundaries under the Robin

22 condition. A governing equation describing spatiotemporal head distributions is employed. The

23 first-order free surface equation with a source term defining a constant recharge rate over a

24 rectangular area is used to depict water table movement. The solution of the model for the head

25 is developed by the methods of Laplace transform and double integral transform. Based on

26 Duhamel's theorem, the present solution is applicable to flow problems accounting for arbitrary

27 time-depending recharge rates. The solution of depth-average head can then be obtained by

28 integrating the head solution to elevation and dividing the result by the aquifer thickness. The

29 use of rectangular aquifer domain has two merits. One is that the integration for estimating the

30 depth-average head can be analytically achieved. The other is that existing solutions based on

31 aquifers of infinite extent can be considered as special cases of the present solution before the

32 time having the aquifer boundary effect on head predictions. With the help of the present

33 solution, the assumption of neglecting the vertical flow effect on the temporal head distribution

34 at an observation point outside a recharge region can be assessed by a dimensionless parameter

35 related to the aquifer horizontal and vertical hydraulic conductivities, initial aquifer thickness,

36 and a shortest distance between the observation point and the edge of the recharge region. The

37 validity of assuming aquifer incompressibility is dominated by the ratio of the aquifer specific

38 yield to its storage coefficient. In addition, a sensitivity analysis is performed to investigate the

39 head response to the change in each of the aquifer parameters.

40 **Keywords:** analytical solution, free surface equation, sensitivity analysis, localized recharge,

41 unconfined aquifers.

1 Introduction

Water table rises due to localized recharge such as rainfall, lakes, and agricultural irrigation into the regional area of the aquifer. Excess recharge may cause soil liquefaction or wet basements of buildings. Groundwater flow behavior induced by recharge is therefore crucial in water resource management. The Boussinesq equation has been extendedly used to describe horizontal flow without the vertical component in unconfined aquifers (e.g., Ireson and Butler, 2013; van der Spek et al., 2013; Yeh and Chang, 2013; Chor and Dias, 2015; Hsieh et al., 2015; Liang and Zhang, 2015; Liang et al., 2015). The equation can be linearized by assuming uniform saturated aquifer thickness for developing its analytical solution. Marino (1967) presented quantitative criteria for the validity of the linearized Boussinesq equation. The criteria are introduced in the next section.

The rate of localized recharge can be a constant for a long term but should be dependent of time for a short term (Rai et al., 2006). An exponentially decaying function of time is usually used for recharge intensity decreasing from a certain rate to an ultimate one. An arbitrary time-depending recharge rate is commonly approximated as the combination of several linear segments of time to develop analytical solutions for water table rise subject to the recharge.

Analytical models accounting for water table rise due to recharge region of an infinite-length strip are reviewed. One-dimensional (1D) flow perpendicular to the strip is considered while the flow along the strip is assumed ignorable. These models deal with aquifers of infinite or finite extent with various types of outer boundary conditions. Hantush (1963) considered an aquifer of infinite extent without a lateral boundary. Rao and Sarma (1980) considered an aquifer of finite extent with two constant-head (also called Dirichlet) boundaries. Later, they developed a solution (Rao and Sarma, 1984) for a finite-extent aquifer between no-flow and constant-head boundaries. Latinopoulos (1986) deliberated on a finite-extent aquifer between two boundaries, one of which is under the Robin condition and the other is under either the

67   Dirichlet or no-flow condition. The recharge rate is treated as a periodical pulse consisting of

68   constant rates for rainy seasons and zero for dry seasons. Bansal and Das (2010) studied an

69   aquifer extending semi-infinitely from a Dirichlet boundary and overlying a sloping impervious

70   base and indicated that the change in groundwater mound induced by strip-shaped recharge

71   region increases with the base slope.

72   A variety of analytical models were presented to describe water table rise for two-

73   dimensional (2D) flow induced by rectangle-shaped recharge into unconfined aquifers. The

74   differences between these solutions are addressed below. Hantush (1967) considered an

75   infinite-extent aquifer with localized recharge having a constant rate. Manglik et al. (1997)

76   handled an arbitrary time-varying rate of recharge into a rectangular aquifer bounded by no-

77   flow stratum. Manglik and Rai (1998) investigated flow behavior based on an irregularly time-

78   varying rate of recharge into a rectangular aquifer with the lateral boundary under the Dirichlet

79   condition. Bruggeman (1999) introduced an analytical solution for steady-state flow induced

80   by localized recharge into a vertical strip aquifer between two Robin boundaries. Chang and

81   Yeh (2007) considered one localized recharge and multiple extraction wells in an anisotropic

82   aquifer overlying an impervious sloping bed. They indicated that the aquifer anisotropy and

83   bottom slope notably influence water table distributions. Bansal and Teloglou (2013) explored

84   the problem of a groundwater mound subject to multiple localized recharges and withdrawal

85   wells in an unconfined aquifer overlying a semi-permeable base. They indicated that

86   groundwater mound rises as decrease in the aquifer hydraulic conductivity.

87   Some articles discussed water table rise near circle-shaped recharge region and thus

88   considered radial groundwater flow which is symmetric to the center of the region. Rai et al.

89   (1998) presented an analytical model describing water table growth subject to an exponentially

90   decaying rate of recharge in a circle-shaped unconfined aquifer with an outer Dirichlet

91   boundary. Illas et al. (2008) considered the same model but a leaky aquifer. They indicated that

92   leakage across the aquifer bottom significantly influences spatiotemporal water table

93   distributions despite a small amount of the leakage. On the other hand, some researchers

94   considered radial flow having the vertical component near a circle-shaped recharge region of

95   an infinite-extent unconfined aquifer. A first-order free surface equation as the top boundary

96   condition of the aquifer is applied to describe water table rise. Zlotnik and Ledder (1992)

97   developed analytical models for describing the distributions of hydraulic head and flow

98   velocity due to constant-rate recharge. They found that models neglecting aquifer

99   compressibility overestimate the magnitudes of the head and flow velocity. Ostendorf et al.

100 (2007) derived an analytical model for head variation due to an exponentially decaying rate of

101 recharge. Predictions of their solution agreed well with the field data obtained in the Plymouth-

102 Carver Aquifer in southeastern Massachusetts given by Hansen and Lapham (1992).

103   Some studies developed a three-dimensional (3D) flow model based on the Laplace

104 equation which neglects the aquifer compressibility effect. Dagan (1967) derived an analytical

105 solution of the velocity potential caused by regional recharge into an unconfined aquifer of

106 infinite thickness. Zlotnik and Ledder (1993) also developed an analytical solution of the same

107 model but considered finite thickness for the unconfined aquifer. Predictions of their solution

108 indicate that groundwater flow are horizontal in the area beyond 150% of the length or width

109 of a rectangular recharge region.

110   It would be informative to summarize the above-mentioned models in Table 1. The

111 solutions of the models are classified according to flow dimensions into 1D, 2D, 3D, and radial

112 flows and further categorized according to aquifer domain, aquifer boundary conditions,

113 recharge region, and recharge rate. The table shows that those solutions assume either no

114 vertical flow or aquifer incompressibility. In addition, the Dirichlet and no-flow conditions

115 considered by some of those solutions are not applicable to a boundary having a semi-

116 permeable stratum, but the Robin condition is. The former two conditions are indeed special

117   cases of the third one.

118   The objective of this paper is to develop a new mathematical model for depicting

119   spatiotemporal hydraulic head distributions subject to localized recharge with an arbitrary time-

120   varying recharge rate in a rectangular-shaped unconfined aquifer. The four boundaries are

121   considered under the Robin condition which can reduce to the Dirichlet or no-flow condition.

122   A governing equation describing 3D transient flow subject to the effect of aquifer

123   compressibility is used. A first-order free surface equation with a source term representing

124   recharge rate is chosen to describe the top boundary condition. The transient head solution of

125   the model is derived by the methods of Laplace transform, double-integral transform, and

126   Duhamel's theorem. The sensitivity analysis based on the present solution is performed to study

127   the head response to the change in each of hydraulic parameters. On the basis of solution's

128   predictions, the effect of the Robin boundaries on time-depending head distributions at

129   observation points is investigated. A quantitative criterion under which the Robin condition

130   reduces to the Dirichlet or no-flow one is provided. In addition, quantitative criteria for the

131   validity of two assumptions of aquifer incompressibility and no vertical flow are provided and

132   errors arising from the assumptions in the hydraulic head are also discussed. Temporal head

133   distributions accounting for transient recharge rates are demonstrated as well.

134

135   **2 Methodology**

136   **2.1 Mathematical model**

137   A mathematical model is developed for describing spatiotemporal hydraulic head

138   distributions induced by localized recharge in a rectangular unconfined aquifer as illustrated in

139   Fig. 1a. The four boundaries of the aquifer are considered under the Robin condition. The

140   aquifer has the widths of l and w in x- and y-directions, respectively. The recharge uniformly

141   distributes over a rectangular region having widths a and b in x- and y-directions, respectively.

142 The lower left corner of the region is designated at (x_1, y_1). The shortest distances measured

143 from the edge of the region to boundaries 1, 2, 3, and 4 are denoted as d_1, d_2, d_3, and d_4,

144 respectively. The shortest distance between the edge of the region and an observation point at

145 (x, y) is defined as $d = \min(\sqrt{(x - x_e)^2 + (y - y_e)^2})$ where (x_e, y_e) is a coordinate on

146 the edge. The initial aquifer thickness is B as shown in Fig. 1b.

147   The governing equation describing 3D transient head distributions in a homogeneous and

148 anisotropic aquifer is expressed as

149 $$K_x \frac{\partial^2 h}{\partial x^2} + K_y \frac{\partial^2 h}{\partial y^2} + K_z \frac{\partial^2 h}{\partial z^2} = S_s \frac{\partial h}{\partial t} \tag{1}$$

150 where t is time, $h(x, y, z, t)$ represents the hydraulic head, K_x, K_y, and K_z are the hydraulic

151 conductivities in x-, y-, and z-directions, respectively, and S_s is the specific storage. The initial

152 static water table is chosen as the reference datum where the elevation head is set to zero. The

153 initial condition is therefore written as

154 $$h = 0 \quad \text{at} \quad t = 0 \tag{2}$$

155 The Robin conditions specified at the four sides of the aquifer are defined as

156 $$\frac{\partial h}{\partial x} - \frac{K_1}{K_x b_1} h = 0 \quad \text{at} \quad x = 0 \tag{3}$$

157 $$\frac{\partial h}{\partial x} + \frac{K_2}{K_x b_2} h = 0 \quad \text{at} \quad x = l \tag{4}$$

158 $$\frac{\partial h}{\partial y} - \frac{K_3}{K_y b_3} h = 0 \quad \text{at} \quad y = 0 \tag{5}$$

159 $$\frac{\partial h}{\partial y} + \frac{K_4}{K_y b_4} h = 0 \quad \text{at} \quad y = w \tag{6}$$

160 where subscripts 1, 2, 3, and 4 represent the boundaries at $x = 0$, $x = l$, $y = 0$, and $y = w$,

161 respectively, and K and b are the hydraulic conductivity and width of the medium at the aquifer

162 boundary, respectively. Note that each of Eqs. (3) − (6) reduces to the Dirichlet condition when

163 b (i.e., b_1, b_2, b_3, or b_4) is set to zero and the no-flow condition when K (i.e., K_1, K_2, K_3, or K_4)

164 is set to zero. The aquifer lies on an impermeable base denoted as

165     $\partial h / \partial z = 0$ at $z = -B$.   (7)

166   The first-order free surface equation describing the response of water table to recharge over the

167   rectangular region can be written as (Zlotnik and Ledder, 1993)

168     $K_z \dfrac{\partial h}{\partial z} + S_y \dfrac{\partial h}{\partial t} = I u_x u_y$ at $z = 0$ (8)

169     $u_x = u(x - x_1) - u(x - x_1 - a)$ (8a)

170     $u_y = u(y - y_1) - u(y - y_1 - b)$ (8b)

171   where S_y is the specific yield, I is a recharge rate, and $u(\ )$ is the unit step function. Equation (8)

172   involves the assumption of $I \ll K_z$ and the simplification from non-uniform saturated aquifer

173   thickness below $z = h$ to uniform one below $z = 0$ (Dagan, 1967). Marino (1967) indicated that

174   the simplification and assumption are valid when the water table rise is smaller than 50% of

175   the initial water table height (i.e., $|h|/B < 0.5$) and the recharge rate is smaller than 20% of the

176   hydraulic conductivity (i.e., $I/K_z < 0.2$). On the other hand, the effect of unsaturated flow above

177   water table on model's predictions can be ignored when $\sigma B \geq 10^3$ where σ is a parameter

178   to define the relative hydraulic conductivity as $k_0 = \exp(-\sigma z)$ in the Richards' equation

179   (Tartakovsky and Neuman, 2007). Tartakovsky and Neuman (2007) achieved agreement on

180   aquifer drawdown evaluated by their analytical solution based on Eq. (1) for saturated flow and

181   Richards' equation for unsaturated flow and by the Neuman (1974) solution based on Eqs. (1)

182   and (8) with $I = 0$ when $\sigma B = 10^3$ (i.e., the case of $\kappa_D = 10^3$ in Fig. 2 in Tartakovsky and

183   Neuman, 2007).

184   Dimensionless variables and parameters are defined as follows

185     $\bar{h} = \dfrac{h}{B}, \quad \bar{x} = \dfrac{x}{d}, \quad \bar{y} = \dfrac{y}{d}, \quad \bar{z} = \dfrac{z}{B}, \quad \bar{l} = \dfrac{l}{d}, \quad \bar{w} = \dfrac{w}{d}, \quad \bar{x}_1 = \dfrac{x_1}{d}, \quad \bar{y}_1 = \dfrac{y_1}{d}, \quad \bar{a} = \dfrac{a}{d}, \quad \bar{b} = \dfrac{b}{d},$

186     $\kappa_z = \dfrac{K_z d^2}{K_x B^2}, \quad \bar{t} = \dfrac{K_x t}{S_s d^2}, \quad \kappa_y = \dfrac{K_y}{K_x}, \quad \kappa_1 = \dfrac{K_1 d}{K_x b_1}, \quad \kappa_2 = \dfrac{K_2 d}{K_x b_2}, \quad \kappa_3 = \dfrac{K_3 d}{K_y b_3}, \quad \kappa_4 = \dfrac{K_4 d}{K_y b_4}, \quad \xi =$

187     $\dfrac{I}{K_z}, \quad \varepsilon = \dfrac{S_y}{S_s B}, \quad \bar{d}_1 = \dfrac{d_1}{d}, \quad \bar{d}_2 = \dfrac{d_2}{d}, \quad \bar{d}_3 = \dfrac{d_3}{d}, \quad \bar{d}_4 = \dfrac{d_4}{d}$ (9)

188   where the overbar denotes a dimensionless symbol. Notice that the variables in the horizontal

189   and vertical directions are divided by d and B, respectively. According to Eq. (9), the

190   mathematical model, Eqs. (1) − (8b), can then be expressed as

191    $\dfrac{\partial^2 \bar{h}}{\partial \bar{x}^2} + \kappa_y \dfrac{\partial^2 \bar{h}}{\partial \bar{y}^2} + \kappa_z \dfrac{\partial^2 \bar{h}}{\partial \bar{z}^2} = \dfrac{\partial \bar{h}}{\partial \bar{t}}$ (10)

192    $\bar{h} = 0$ at $\bar{t} = 0$ (11)

193    $\dfrac{\partial \bar{h}}{\partial \bar{x}} - \kappa_1 \bar{h} = 0$ at $\bar{x} = 0$ (12)

194    $\dfrac{\partial \bar{h}}{\partial \bar{x}} + \kappa_2 \bar{h} = 0$ at $\bar{x} = \bar{l}$ (13)

195    $\dfrac{\partial \bar{h}}{\partial \bar{y}} - \kappa_3 \bar{h} = 0$ at $\bar{y} = 0$ (14)

196    $\dfrac{\partial \bar{h}}{\partial \bar{y}} + \kappa_4 \bar{h} = 0$ at $\bar{y} = \bar{w}$ (15)

197    $\partial \bar{h} / \partial \bar{z} = 0$ at $\bar{z} = -1$ (16)

198    $\dfrac{\partial \bar{h}}{\partial \bar{z}} + \dfrac{\varepsilon}{\kappa_z} \dfrac{\partial \bar{h}}{\partial \bar{t}} = \xi \bar{u}_x \bar{u}_y$ at $\bar{z} = 0$ (17)

199    $\bar{u}_x = u(\bar{x} - \bar{x}_1) - u(\bar{x} - \bar{x}_1 - \bar{a})$ (17a)

200    $\bar{u}_y = u(\bar{y} - \bar{y}_1) - u(\bar{y} - \bar{y}_1 - \bar{b})$.   (17b)

201

202   **2.2 Analytical solution**

203   The mathematical model, Eqs. (10) − (17b), can be solved by the methods of Laplace

204   transform and double-integral transform. The former transform converts $\bar{h}(\bar{x}, \bar{y}, \bar{z}, \bar{t})$ into

205    $\tilde{h}(\bar{x}, \bar{y}, \bar{z}, p)$, $\partial \bar{h} / \partial \bar{t}$ into $p\tilde{h} - \bar{h}|_{\bar{t}=0}$, and $\xi \bar{u}_x \bar{u}_y$ into $\xi \bar{u}_x \bar{u}_y / p$ where p is the Laplace

206   parameter and $\bar{h}|_{\bar{t}=0}$ equals zero in Eq. (11). After taking the transform, the model become a

207   boundary value problem expressed as

208    $\dfrac{\partial^2 \tilde{h}}{\partial \bar{x}^2} + \kappa_y \dfrac{\partial^2 \tilde{h}}{\partial \bar{y}^2} + \kappa_z \dfrac{\partial^2 \tilde{h}}{\partial \bar{z}^2} = p\tilde{h}$ (18)

209   with boundary conditions $\partial \tilde{h} / \partial \bar{x} - \kappa_1 \tilde{h} = 0$ at $\bar{x} = 0$, $\partial \tilde{h} / \partial \bar{x} + \kappa_2 \tilde{h} = 0$ at $\bar{x} = \bar{l}$, $\tilde{h} /$

210    $\partial \bar{y} - \kappa_3 \tilde{h} = 0$ at $\bar{y} = 0$, $\tilde{h} / \partial \bar{y} + \kappa_4 \tilde{h} = 0$ at $\bar{y} = \bar{w}$, $\partial \tilde{h} / \partial \bar{z} = 0$ at $\bar{z} = -1$, and $\partial \tilde{h} /$

211      $\partial \bar{z} + \varepsilon p \tilde{h}/\kappa_z = \xi \bar{u}_x \bar{u}_y/p$ at $\bar{z} = 0$. We then apply the properties of the double-integral

212   transform to the problem. One can refer to the definition in Latinopoulos (1985, Table I, aquifer

213   type 1). The transform turns $\tilde{h}(\bar{x}, \bar{y}, \bar{z}, p)$ into $\hat{h}(\alpha_m, \beta_n, \bar{z}, p)$, $\partial^2 \tilde{h}/\partial \bar{x}^2 + \kappa_y(\partial^2 \tilde{h}/\partial \bar{y}^2)$

214   into $-(\alpha_m^2 + \kappa_y \beta_n^2)\hat{h}$ where $(m, n) \in 1, 2, 3, \dots \infty$, and eigenvalues α_m and β_n are the

215   positive roots of the following equations that

216      $\tan(\bar{l}\alpha_m) = \frac{\alpha_m(\kappa_1 + \kappa_2)}{\alpha_m^2 - \kappa_1 \kappa_2}$ (19)

217   and

218      $\tan(\bar{w}\beta_n) = \frac{\beta_n(\kappa_3 + \kappa_4)}{\beta_n^2 - \kappa_3 \kappa_4}$.   (20)

219   In addition, $\bar{u}_x \bar{u}_y$ defined in Eqs. (17a) and (17b) is transformed into $U_m U_n$ given by

220      $U_m = \dfrac{\sqrt{2} V_m}{\sqrt{\kappa_1 + (\alpha_m^2 + \kappa_1^2)[\bar{l} + \kappa_2/(\alpha_m^2 + \kappa_2^2)]}}$ (21)

221      $U_n = \dfrac{\sqrt{2} V_n}{\sqrt{\kappa_3 + (\beta_n^2 + \kappa_3^2)[\bar{w} + \kappa_4/(\beta_n^2 + \kappa_4^2)]}}$ (22)

222   with

223      $V_m = \{\kappa_1[\cos(\alpha_m \bar{x}_1) - \cos(\alpha_m \chi)] - \alpha_m[\sin(\alpha_m \bar{x}_1) - \sin(\alpha_m \chi)]\}/\alpha_m$ (23)

224      $V_n = \{\kappa_3[\cos(\beta_n \bar{y}_1) - \cos(\beta_n \psi)] - \beta_n[\sin(\beta_n \bar{y}_1) - \sin(\beta_n \psi)]\}/\beta_n$ (24)

225   where $\chi = \bar{x}_1 + \bar{a}$ and $\psi = \bar{y}_1 + \bar{b}$.

226   Equation (18) then reduces to an ordinary differential equation as

227      $\kappa_z \dfrac{\partial^2 \hat{h}}{\partial \bar{z}^2} - (p + \alpha_m^2 + \kappa_y \beta_n^2)\hat{h} = 0$ (25)

228   Two boundary conditions are expressed, respectively, as

229      $\partial \hat{h}/\partial \bar{z} = 0$ at $\bar{z} = -1$ (26)

230   and

231      $\dfrac{\partial \hat{h}}{\partial \bar{z}} + \dfrac{\varepsilon p}{\kappa_z}\hat{h} = \dfrac{\xi}{p} U_m U_n$ at $\bar{z} = 0$.   (27)

232   Solving Eq. (25) with Eqs. (26) and (27) results in

233 $\hat{h}(\alpha_m, \beta_n, \bar{z}, p) = \frac{\xi U_m U_n \cosh[(1+\bar{z})\lambda]}{p(p\varepsilon\kappa_z \cosh\lambda + \kappa_z\lambda \sinh\lambda)}$ (28)

234 where

235 $\lambda = \sqrt{(p + \alpha_m^2 + \kappa_y\beta_n^2)/\kappa_z}.$ (29)

236 Inverting Eq. (28) to the space and time domains gives rise to the analytical solution that

237 $\bar{h}(\bar{x}, \bar{y}, \bar{z}, \bar{t}) = \xi \sum_{m=1}^{\infty} \sum_{n=1}^{\infty} (\phi_{m,n} + \phi_{0,m,n} + \sum_{j=1}^{\infty} \phi_{j,m,n})F_m F_n U_m U_n$ (30)

238 with

239 $\phi_{m,n} = \frac{\cosh[(1+\bar{z})\lambda_{m,n}]}{\kappa_z \lambda_{m,n} \sinh\lambda_{m,n}}$ (30a)

240 $\phi_{0,m,n} = -2\lambda_{0,m,n}\cosh[(1+\bar{z})\lambda_{0,m,n}]\exp(-\gamma_{0,m,n}\bar{t})/\eta_{0,m,n}$ (30b)

241 $\phi_{j,m,n} = -2\lambda_{j,m,n}\cos[(1+\bar{z})\lambda_{j,m,n}]\exp(-\gamma_{j,m,n}\bar{t})/\eta_{j,m,n}$ (30c)

242 $\eta_{0,m,n} = \gamma_{0,m,n}[(1+2\varepsilon\kappa_z)\lambda_{0,m,n}\cosh\lambda_{0,m,n} + (1-\varepsilon\gamma_{0,m,n})\sinh\lambda_{0,m,n}]$ (30d)

243 $\eta_{j,m,n} = \gamma_{j,m,n}[(1+2\varepsilon\kappa_z)\lambda_{j,m,n}\cos\lambda_{j,m,n} + (1-\varepsilon\gamma_{j,m,n})\sin\lambda_{j,m,n}]$ (30e)

244 $\lambda_{m,n} = \sqrt{f_{m,n}/\kappa_z};\ \gamma_{0,m,n} = f_{m,n} - \kappa_z\lambda_{0,m,n}^2;\ \gamma_{j,m,n} = f_{m,n} + \kappa_z\lambda_{j,m,n}^2$ (30f)

245 $f_{m,n} = \alpha_m^2 + \kappa_y\beta_n^2$ (30g)

246 $F_m = \frac{\sqrt{2}[\alpha_m \cos(\alpha_m\bar{x}) + \kappa_1 \sin(\alpha_m\bar{x})]}{\sqrt{\kappa_1 + (\alpha_m^2 + \kappa_1^2)[\bar{l} + \kappa_2/(\alpha_m^2 + \kappa_2^2)]}}$ (30h)

247 $F_n = \frac{\sqrt{2}[\beta_n \cos(\beta_n\bar{y}) + \kappa_3 \sin(\beta_n\bar{y})]}{\sqrt{\kappa_3 + (\beta_n^2 + \kappa_3^2)[\bar{w} + \kappa_4/(\beta_n^2 + \kappa_4^2)]}}$ (30i)

248 where $j \in 1, 2, 3, \ldots\infty$ and eigenvalues $\lambda_{0,m,n}$ and $\lambda_{j,m,n}$ are determined, respectively, by the

249 following equations that

250 $\tan\lambda_{j,m,n} = -\varepsilon(f_{m,n} + \kappa_z\lambda_{j,m,n}^2)/\lambda_{j,m,n}$ (31)

251 and

252 $\frac{-\varepsilon\kappa_z\lambda_{0,m,n}^2 + \lambda_{0,m,n} + \varepsilon f_{m,n}}{\varepsilon\kappa_z\lambda_{0,m,n}^2 + \lambda_{0,m,n} - \varepsilon f_{m,n}} = \exp(2\lambda_{0,m,n}).$ (32)

253 Notice that Eqs. (19), (20), and (31) have infinite positive roots owing to the trigonometric

254   function tan( ) while Eq. (32) has only one positive root. The method to find α_m, β_n, $\lambda_{j,m,n}$

255   and $\lambda_{0,m,n}$ is introduced in Sect. 2.3. One can refer to Appendix A for the derivation of Eq.

256   (30). The first term on the right-hand side (RHS) of Eq. (30) is a double series expanded by

257   α_m and β_n. The series converges within a few terms because the power of α_m (or β_n) in the

258   denominator of $\phi_{m,n}$ in Eq. (30a) is two more than that in the nominator. The second term on

259   the RHS of Eq. (30) is a double series expanded by α_m and β_n, and the third term is a triple

260   series expanded by α_m, β_n, and $\lambda_{j,m,n}$. They converge very fast due to exponential functions

261   in Eqs. (30b) and (30c). Consider $(m, n) \in (1, 2, …, N = 30)$ and $j \in (1, 2, …, N_j = 15)$ for the

262   default values of dimensionless parameters and variables in Table 2 for calculation. The number

263   of terms in one or the other double series is $30 \times 30 = 900$ and in the triple series is $30 \times 30 \times$

264      $15 = 13500$. The total number is therefore $900 \times 2 + 13500 = 15300$. We apply Mathematica

265   FindRoot routine to obtain the values of α_m, β_n, and $\lambda_{j,m,n}$ and Sum routine to compute the

266   double and triple series. It takes about 8 seconds to finish calculation for $\bar{t} = 10^5$ by a

267   personal computer with Intel Core i5-4590 3.30 GHz processor and 8 GB RAM. In addition,

268   the series is considered to converge when the absolute value of the last term in the double series

269   of $\phi_{m,n}$ is smaller than 10^{-20} (i.e., $10^{-50} < 10^{-20}$ in this case). That value in the other double or

270   triple series may be even smaller than 10^{-50} due to exponential decay.

271   The use of finite aquifer domain has two merits. One is that the solution of depth-average

272   head, defined as $\int_{-1}^{0} \bar{h}(\bar{x}, \bar{y}, \bar{z}, \bar{t}) \, d\bar{z}$, can be analytically integrated. The integration variable $\bar{z}$

273   appears only in the functions of $\cosh[(1 + \bar{z})\lambda_{m,n}]$ in Eq. (30a), $\cosh[(1 + \bar{z})\lambda_{0,m,n}]$ in Eq.

274   (30b) and $\cos[(1 + \bar{z})\lambda_{j,m,n}]$ in Eq. (30c). The solution of depth-average head therefore

275   equals Eq. (30) where these three functions are replaced by $\sinh \lambda_{m,n} / \lambda_{m,n}$, $\sinh \lambda_{0,m,n} /$

276      $\lambda_{0,m,n}$, and $\sin \lambda_{j,m,n} / \lambda_{j,m,n}$, respectively. The other is that the present solution is applicable

277   to head predictions in aquifers of infinite extent before the dimensionless time to have lateral

278 aquifer boundary effect on the predictions. Wang and Yeh (2008) reported a time criterion

279 defined as $\bar{t}_{cr} = 0.03(1 + \varepsilon)\bar{R}^2$ where $\bar{R} = R/d$ denotes a shortest dimensionless distance

280 from the lateral boundary to the edge of the recharge region. This criterion is, in effect, a

281 boundary-effect time when the hydraulic head is affected by the aquifer boundary. Existing

282 solutions based on aquifers of infinite extent can therefore be considered as special cases of the

283 present solution before the boundary-effect time.

284

285 **2.3 Calculation of eigenvalues**

286   The eigenvalues α_m, β_n, $\lambda_{j,m,n}$, and $\lambda_{0,m,n}$ can be determined by Newton's method

287 with initial guess values (IGVs) set to be the vertical asymptotes of the functions on the left-

288 hand side (LHS) of Eqs. (19), (20), (31), and (32), respectively. Hence, IGVs for α_m are $\alpha' +$

289 δ if $\alpha' < (\kappa_1\kappa_2)^{1/2}$ and $\alpha' - \delta$ if $\alpha' > (\kappa_1\kappa_2)^{1/2}$ where $\alpha' = (2m - 1)\pi/(2\bar{l})$ and δ

290 is a small value of 10^{-8} to avoid being right at the vertical asymptotes. Similarly, IGVs for

291 β_n are $\beta' + \delta$ if $\beta' < (\kappa_3\kappa_4)^{1/2}$ and $\beta' - \delta$ if $\beta' > (\kappa_3\kappa_4)^{1/2}$ where $\beta' = (2n - 1)\pi/$

292 $(2\bar{w})$. In addition, IGVs for $\lambda_{j,m,n}$ are $(2j - 1)\pi/2 + \delta$, and IGV for $\lambda_{0,m,n}$ is $\delta +$

293 $\left[\left(1 + 4\kappa_z f_{m,n}\varepsilon^2\right)^{1/2} - 1\right]/(2\varepsilon\kappa_z)$ obtained by setting the denominator of the LHS function

294 of Eq. (32) to be zero and solving the resultant equation.

295

296 **2.4 Solution for time-varying recharge rate**

297   The present solution, Eq. (30), is applicable to arbitrary time-depending recharge rates on

298 the basis of Duhamel's theorem expressed as (e.g., Bear, 1979, p. 158)

299 $\bar{h}_{It} = \bar{h}_{I0} + \int_0^{\bar{t}} \frac{\partial \xi_t(\tau)}{\partial \tau} \bar{h}(\bar{t} - \tau)/\xi \, d\tau$ (33)

300 where $\bar{h}_{It}$ signifies a dimensionless head solution for a time-depending recharge rate $\xi_t(\tau)$

301 with $\bar{t}$ replaced by τ, $\bar{h}_{I0}$ is Eq. (30) in which ξ is replaced by $\xi_t(0)$, and $\bar{h}(\bar{t} - \tau)$ is also

302 Eq. (30) with $\bar{t}$ replaced by $\bar{t} - \tau$. If Eq. (33) is not integrable, it can be discretized as (Singh,

303 2005)

304 $\quad \bar{h}_N = \sum_{i=1}^{N} \frac{\Delta\xi_i}{\Delta\bar{t}} \eta(N - i + 1)$ (34)

305 with

306 $\quad \Delta\xi_i = \xi_i - \xi_{i-1}$ (34a)

307 $\quad \eta(M) = \int_0^{\bar{t}} \bar{h}(M\Delta\bar{t} - \tau)d\tau$ (34b)

308 where $\bar{h}_N$ represents a numerical result of dimensionless head $\bar{h}$ at $\bar{t} = \Delta\bar{t} \times N$, $\Delta\bar{t}$ is a

309 dimensionless time step, ξ_i and ξ_{i-1} are dimensionless recharge rates at $\bar{t} = \Delta\bar{t} \times i$ and

310 $\bar{t} = \Delta\bar{t} \times (i - 1)$, respectively, and $\eta(M)$, called ramp kernel, depends on Eq. (30) in which

311 $\bar{t}$ is replaced by $M\Delta\bar{t} - \tau$. The integration result of Eq. (34b) can be denoted as Eq. (30) where

312 $\phi_{m,n}$ is replaced by $\phi_{m,n}\bar{t}$ and two exponential terms in Eqs. (30b) and (30c) are replaced,

313 respectively, by $\quad \exp(-M\gamma_{0,m,n}\Delta\bar{t})\left[-1 + \exp(\gamma_{0,m,n}\Delta\bar{t})\right]/\gamma_{0,m,n}$ and

314 $\exp(-M\gamma_{j,m,n}\Delta\bar{t})\left[-1 + \exp(\gamma_{j,m,n}\Delta\bar{t})\right]/\gamma_{j,m,n}$.

315

316 **2.5 Sensitivity analysis**

317 The sensitivity analysis is administered to assess the change in the hydraulic head in

318 response to the change in each of the hydraulic parameters. The normalized sensitivity

319 coefficient of the hydraulic head to a specific parameter can be expressed as

320 $\quad S_{c,t} = \frac{\partial h/B}{\partial P_c/P_c} = \frac{\partial \bar{h}}{\partial P_c/P_c}$ (35)

321 where P_c is the c-th parameter in the present solution, $S_{c,t}$ is the coefficient at a time to the c-

322 th parameter, and $\bar{h}$ is the present solution, Eq. (30). The derivative in Eq. (35) can be

323 approximated as

324 $\quad S_{c,t} = \frac{\bar{h}(P_c + \Delta P_c) - \bar{h}(P_c)}{\Delta P_c/P_c}$ (36)

325   where ΔP_c is an increment chosen as $10^{-3}P_c$ (Yeh et al., 2008).

326

327   **3 Results and discussion**

328   Previous articles have discussed groundwater mounds in response to localized recharge

329   into aquifers with various hydraulic parameters (e.g., Dagan, 1967; Rao and Sarma, 1980;

330   Latinopoulos, 1986; Manglik et al., 1997; Manglik and Rai, 1998; Rai et al., 1998; Chang and

331   Yeh, 2007; Illas et al., 2008; Bansal and Das, 2010; Bansal and Teloglou, 2013). Flow velocity

332   fields below groundwater mounds have also been analyzed (Zlotnik and Ledder, 1992; Zlotnik

333   and Ledder, 1993). This section therefore focuses on the transient behavior of hydraulic head

334   at an observation point with the aid of the present solution. The default values of the parameters

335   and variables for calculation are noted in Table 2. In Sect. 3.1, transient head distributions

336   subject to Dirichlet, no-flow and Robin boundary conditions are compared. In Sect. 3.2, the

337   effect of vertical flow on the head distribution is investigated. In Sect. 3.3, errors arising from

338   assuming aquifer incompressibility (i.e., $S_s = 0$) to develop analytical solutions are discussed.

339   In Sect. 3.4, the response of the hydraulic head to transient recharge rates based on Eq. (33) is

340   demonstrated. In Sect. 3.5, the sensitivity analysis defined by Eq. (36) is performed.

341

342   **3.1 Effect of lateral boundary**

343   The Robin condition can become the Dirichlet or no-flow one, depending on the

344   magnitudes of $\kappa_1 \bar{d}_1$ for Eq. (12), $\kappa_2 \bar{d}_2$ for Eq. (13), $\kappa_3 \bar{d}_3$ for Eq. (14), and $\kappa_4 \bar{d}_4$ for Eq.

345   (15). We consider a symmetrical aquifer system with $\bar{l} = \bar{w} = 22$, $\bar{d}_1 = \bar{d}_2 = \bar{d}_3 = \bar{d}_4 =$

346   10 and $\kappa_1 = \kappa_2 = \kappa_3 = \kappa_4$. The magnitudes of $\kappa_1 \bar{d}_1$, $\kappa_2 \bar{d}_2$, $\kappa_3 \bar{d}_3$ and $\kappa_4 \bar{d}_4$ are the same

347   and defined as κ. The curves of $\bar{h}$ versus $\bar{t}$ plotted by the present solution, Eq. (30), for $\kappa =$

348   10^{-3}, 10^{-2}, 10^{-1}, 1, 10, 100, and 200 are shown in Fig. 2. The curves $\bar{h}$ versus $\bar{t}$ are plotted

349   from Manglik et al. (1997) solution with the no-flow condition (i.e., $\kappa = 0$), Manglik and Rai

350　　　(1998) solution with the Dirichlet condition (i.e., $\kappa \to \infty$), and the present solution with the

351　　　Robin condition. Before $\bar{t} = 10^4$, these curves give the same magnitude of $\bar{h}$ at a fixed

352　　　dimensionless time $\bar{t}$ since the lateral aquifer boundary has been beyond the place where

353　　　groundwater is affected by localized recharge. After $\bar{t} = 10^4$, the curves for the cases of $\kappa =$

354　　　10^{-2}, 10^{-1}, 1, 10, and 100 deviate from each other gradually as time increases. A larger

355　　　magnitude of κ between $\kappa = 10^{-2}$ and $\kappa = 100$ causes a smaller $\bar{h}$ at a fixed $\bar{t}$. On the other

356　　　hand, the present solution for the cases of $\kappa = 10^{-3}$ and 10^{-2} agrees well with Manglik et al.

357　　　(1997) solution based on $\kappa = 0$ and that for the cases of $\kappa = 100$ and 200 predicts the same result

358　　　as Manglik and Rai (1998) solution based on $\kappa \to \infty$. We may reasonably conclude that the

359　　　Robin condition reduces to the no-flow one when $\kappa \leq 10^{-2}$ and the Dirichlet one when $\kappa \geq 100$.

360

361　　　**3.2 Effect of vertical flow**

362　　　　　Dimensionless parameter κ_z (i.e., $K_z d^2/(K_x B^2)$) dominates the effect of vertical flow

363　　　on transient head distributions at an observation point. Consider $\kappa_1 \bar{d}_1 = \kappa_2 \bar{d}_2 = \kappa_3 \bar{d}_3 =$

364　　　$\kappa_4 \bar{d}_4 = 100$ for lateral aquifer boundaries under the Dirichlet condition as discussed in Sect.

365　　　3.1. The temporal distributions of $\bar{h}$ predicted by the present solution, Eq. (30), with $\kappa_z =$

366　　　0.01, 0.1, 1, and 10 are demonstrated in Fig. 3. The temporal distribution of $\bar{h}$ predicted by

367　　　Manglik and Rai (1998) solution based on 2D flow without the vertical component is taken in

368　　　order to address the effect of vertical flow. The figure reveals that $\bar{h}$ increases with κ_z when

369　　　$\kappa_z \leq 1$. The difference in $\bar{h}$ predicted by both solutions indicates the vertical flow effect. The

370　　　Manglik and Rai (1998) solution obviously overestimates the head. The vertical flow prevails,

371　　　and its effect should be taken into account when $\kappa_z < 1$, indicating a thick aquifer, a small

372　　　ratio of K_z/K_x, and/or an observation point near a recharge region. On the other hand, the present

373　　　solution for the cases of $\kappa_z = 1$ and 10 agrees well with Manglik and Rai (1998) solution,

374　　　indicating that the vertical flow effect is ignorable when $\kappa_z \geq 1$. We can recognize from the

16

375   agreement that existing solutions neglecting the vertical flow effect give good predictions when

376   $\kappa_z \geq 1$.

377

378   **3.3 Effect of specific storage**

379   Some of existing models use the Laplace equation as a governing equation with assuming

380   $S_s = 0$ (e.g., Singh, 1976; Schmitz and Edenhofer, 1988; Zlotnik and Ledder, 1993). The

381   assumption is valid when ε (i.e., $S_y/(S_sB)$) is larger than a certain value. This section quantifies

382   the value. The Zlotnik and Ledder (1993) model based on 3D Laplace equation, Eq. (1) with

383   $S_s = 0$, is taken for comparison with the present model using Eq. (1) with $S_s \neq 0$. The

384   dimensionless variables of s, x, y, z, t, X, and Y in their model are replaced by $\bar{h}/\xi$, $(\kappa_z)^{1/2}\bar{x}$,

385   $(\kappa_z)^{1/2}\bar{y}$, $\bar{z}$, $\kappa_z\bar{t}/\varepsilon$, $(\kappa_z)^{1/2}\bar{a}$, and $(\kappa_z)^{1/2}\bar{b}$, respectively, for ease of comparisons. Consider

386   the cases of $\kappa_z = 10^{-2}$ for an observation point located at a 3D flow area and $\kappa_z = 10$ for the point

387   located at a 2D flow area as discussed in Sect. 3.2. The assumption can be assessed through the

388   comparison in the dimensionless heads predicted by both solutions for $\varepsilon = 1$, 10, 10^2, and 10^3

389   as shown in Fig. 4a for $\kappa_z = 10^{-2}$ and Fig. 4b for $\kappa_z = 10$. The present solution predicts a steady-

390   state $\bar{h}$ of 0.054 in Fig. 4a and 0.074 in Fig. 4b after certain times due to lateral Dirichlet

391   boundaries (i.e., $\kappa_1\bar{d}_1 = \kappa_2\bar{d}_2 = \kappa_3\bar{d}_3 = \kappa_4\bar{d}_4 = 100$) as discussed in Sect. 3.1. In contrast,

392   their solution predicts $\bar{h}$ which increases with $\bar{t}$ due to the absence of lateral boundaries.

393   When $\varepsilon = 1$ and 10, both solutions give different values of $\bar{h}$ for both cases of $\kappa_z = 10^{-2}$ and

394   $\kappa_z = 10$ before $\bar{t} = 100$, indicating that the assumption of $S_s = 0$ causes inaccurate $\bar{h}$. When ε

395   $= 10^2$ and 10^3, both solutions predict very close results of $\bar{h}$ for both cases before the time of

396   approaching steady-state $\bar{h}$. These results lead to the conclusion that the assumption of $S_s = 0$

397   is valid when $\varepsilon \geq 100$ for 3D and 2D flow cases.

398

399   **3.4 Transient recharge rate**

400   Most articles (e.g., Rai et al., 1998; Chang and Yeh, 2007; Illas et al., 2008; Bansal and

401   Teloglou, 2013) define a transient recharge rate as $I_t(t) = I_1 + I_0 \exp(-rt)$ (i.e., $\xi_t(\bar{t}) =$

402     $\xi_1 + \xi_0 \exp(-\gamma\bar{t})$ for a dimensionless rate) where $\xi_t = I_t/K_z$, $\xi_1 = I_1/K_z$, $\xi_0 = I_0/K_z$,

403     $\gamma = rS_s d^2/K_x$, and r is a decay constant. The rate exponentially declines from an initial value

404   of $I_1 + I_0$ to an ultimate one of I_1. The present solution, Eq. (30), can be applied for the

405   response of the head to the transient rate based on Eq. (33). Substituting $\partial\xi_t(\tau)/\partial\tau =$

406     $-\gamma\xi_0 \exp(-\gamma\tau)$ into Eq. (33) and integrating the result for τ from $\tau = 0$ to $\tau = \bar{t}$ yields

407     $\bar{h}_{I0}$ plus Eq. (30) where ξ in Eq. (30), $\phi_{m,n}$ in Eq. (30a), $\exp(-\gamma_{0,m,n}\bar{t})$ in (30b), and

408     $\exp(-\gamma_{j,m,n}\bar{t})$ in (30c) are replaced by ξ_0, $\phi_{m,n}[\exp(-\gamma\bar{t}) - 1]$, $\gamma[\exp(-\gamma\bar{t}) -$

409     $\exp(\gamma_{0,m,n}\bar{t})]/(\gamma_{0,m,n} + \gamma)$, and $\gamma[\exp(-\gamma\bar{t}) - \exp(\gamma_{j,m,n}\bar{t})]/(\gamma_{j,m,n} + \gamma)$, respectively.

410   Similarly, Zlotnik and Ledder (1993) solution can also be used to obtain the head subject to the

411   transient rate by substituting it into Eq. (33) and then integrating the result using numerical

412   approaches. Now, we consider Ramana et al. (1995) solution depicting 2D flow induced by the

413   transient rate in rectangular aquifers with the lateral boundaries under the Dirichlet condition.

414   Figure 5 shows the temporal distributions of $\bar{h}$ for the transient rate predicted by these three

415   solutions when $\kappa_z = 1$, $\kappa = 100$, and $\varepsilon = 100$. The present solution agrees well with

416   Ramana et al. (1995) solution. We can recognize from the agreement that, even for transient

417   rates, the Robin condition reduces to the Dirichlet one when $\kappa \geq 100$ (i.e., $\kappa_1\bar{d}_1 = \kappa_2\bar{d}_2 =$

418     $\kappa_3\bar{d}_3 = \kappa_4\bar{d}_4 = 100$) as discussed in Sect. 3.1 and the vertical flow effect is ignorable when

419     $\kappa_z \geq 1$ as discussed in Sect. 3.2. Moreover, agreement on $\bar{h}$ estimated by the present solution

420   and Zlotnik and Ledder (1993) solution before $\bar{t} = 3 \times 10^3$ will make clear that, even for

421   transient rates, assuming aquifer incompressibility (i.e., $S_s = 0$) is valid when $\varepsilon \geq 100$ as

422   discussed in Sect. 3.3.

423

424   **3.5 Sensitivity analysis**

425   Consider point A of (555 m, 500 m, −10 m) at a 3D flow region (i.e., $\kappa_z < 1$) and point

426   B of (800 m, 500 m, −10 m) at a 2D flow region (i.e., $\kappa_z \geq 1$) as discussed in Sect. 3.2.

427   Localized recharge distributes over the square area of 450 m ≤ x ≤ 550 m and 450 m ≤ y ≤ 550

428   m. The distance d herein is set to 5 m for point A and 250 m for point B. The aquifer system is

429   of isotropy with $K_x = K_y$ and symmetry with $K_1 = K_2 = K_3 = K_4$ for conciseness. The sensitivity

430   analysis is performed by Eq. (36) to investigate the responses of the hydraulic heads at these

431   two points to the change in each of a, b, S_s, S_y, K_x (or K_y), K_z, and K_1 (or K_2, K_3, and K_4). The

432   curves of the normalized sensitivity coefficient $S_{c,t}$ versus t for these seven parameters are

433   shown in Fig. 6a for point A and Fig. 6b for point B. The figure shows that the hydraulic heads

434   at both points are more sensitive to the changes in a, b, K_x, and S_y than those in the others. This

435   may indicate that a flow model should include at least these four parameters. The figure also

436   shows that the heads at points A and B are insensitive to the change in K_1 because of $\kappa_1 \bar{d}_1 =$

437   4500 > 100 as discussed in Sect. 3.1. In addition, $S_{c,t}$ to K_z for point A is nonzero after $t = 0.4$

438   day due to $\kappa_z = 6.25 \times 10^{-3} < 1$ as discussed in Sect. 3.2. In contrast, $S_{c,t}$ to K_z for point B

439   is very close to zero over the entire period because of $\kappa_z = 15.625 > 1$. Moreover, the heads

440   at points A and B are insensitive to the change in S_s due to $\varepsilon = 500 > 100$ as discussed in Sect.

441   3.3.

442

443   **4 Conclusions**

444   A mathematical model is developed to depict spatiotemporal head distributions induced

445   by localized recharge with an arbitrary time-varying rate in a rectangular unconfined aquifer

446   bounded by Robin boundaries with different hydraulic parameters. A governing equation for

447   3D flow is considered. A first-order free surface equation with a source term representing the

448   recharge is employed for describing the water table movement. The analytical head solution of

449   the model is obtained by applying the Laplace transform, the double-integral transform, and

450   Duhamel's theorem. The use of rectangular aquifer domain leads to two merits. One is that the

451   integration for the solution of the depth-average head can be analytically done. The other is

452   that existing solutions based on aquifers of infinite extent are special cases of the present

453   solution when the recharge time is less than the boundary-effect time. The present solution is

454   applicable under the conditions of aquifer homogeneity, $|h|/B < 0.5$, $I/K_z < 0.2$, and $\sigma B \geq$

455   10^3 due to Eq. (8) neglecting the effect of unsaturated flow above water table (Marino, 1967;

456   Tartakovsky and Neuman, 2007). The sensitivity analysis is performed to explore the response

457   of the head to the change in each of hydraulic parameters. With the aid of the present solution,

458   the following conclusions can be drawn:

459   1. In respect of affecting $\bar{h}$ at observation points, the Robin condition specified at $\bar{x} = 0$

460   reduces to the Dirichlet one when $\kappa_1 \bar{d}_1 \geq 100$ (i.e., $K_1 d_1/(K_x b_1) \geq 100$) and no-flow one

461   when $\kappa_1 \bar{d}_1 \leq 10^{-2}$. The quantitative criteria for $\kappa_1 \bar{d}_1$ are applicable to $\kappa_2 \bar{d}_2$, $\kappa_3 \bar{d}_3$, and

462         $\kappa_4 \bar{d}_4$ for the Robin conditions specified at $\bar{x} = \bar{l}$, $\bar{y} = 0$, and $\bar{y} = \bar{w}$, respectively.

463   2. The vertical flow causes significant decrease in the hydraulic head at an observation point

464   when $\kappa_z < 1$ (i.e., $K_z d^2/(K_x B^2) < 1$). When $\kappa_z \geq 1$, the effect of vertical flow on the head is

465   ignorable, and conventional models considering 2D flow without the vertical component

466   can therefore predict accurate results.

467   3. The 3D Laplace equation based on the assumption of $S_s = 0$ can be regarded as a flow

468   governing equation when $\varepsilon \geq 100$ (i.e., $S_y/(S_s B) \geq 100$) for the whole aquifer domain.

469   Otherwise, head predictions based on the Laplace equation are overestimated.

470   4. The abovementioned conclusions are also applicable to problems of groundwater flow

471   subject to recharge with arbitrary time-varying rates.

472

473   **Appendix A: Derivation of Eq. (30)**

474   Let us start with function $G(p)$ from Eq. (28) that

475    $G(p) = \dfrac{\cosh[(1+\bar{z})\lambda]}{p(p\varepsilon\kappa_z\cosh\lambda+\kappa_z\lambda\sinh\lambda)}$ (A1)

476   with

477    $\lambda = \sqrt{(p + f_{m,n})/\kappa_z}$ (A2)

478   where $f_{m,n} = \alpha_m^2 + \kappa_y\beta_n^2$. Equation (A1) is a single-value function to p in the complex plane

479   because satisfying $G(p^+) = G(p^-)$ where p^+ and p^- are the polar coordinates defined,

480   respectively, as

481    $p^+ = r_a\exp(i\theta) - f_{m,n}$ (A3)

482   and

483    $p^- = r_a\exp[i(\theta - 2\pi)] - f_{m,n}$ (A4)

484   where r_a represents a radial distance from the origin at $p = -f_{m,n}$, $i = \sqrt{-1}$ is the imaginary

485   unit, and θ is an argument between 0 and 2π. Substitute $p = p^+$ in Eq. (A3) into Eq. (A2),

486   and we have

487    $\lambda = \sqrt{r_a/\kappa_z}\,\exp(i\theta/2) = \sqrt{r_a/\kappa_z}\,[\cos(\theta/2) + i\sin(\theta/2)]$ (A5)

488   Similarly, we can have

489    $\lambda = \sqrt{r_a/\kappa_z}\,\exp[i(\theta - 2\pi)/2] = -\sqrt{r_a/\kappa_z}\,[\cos(\theta/2) + i\sin(\theta/2)]$ (A6)

490   after p in Eq. (A2) is replaced by p^- in Eq. (A4). Substitution of Eqs. (A3) and (A5) into Eq.

491   (A1) yields the same result as that obtained by substituting Eqs. (A4) and (A6) into Eq. (A1),

492   indicating that Eq. (A1) is a single-value function without branch cut and its inverse Laplace

493   transform equals the sum of residues for poles in the complex plane.

494   The residue for a simple pole can be formulated as

495    $Res = \lim\limits_{p\to\varphi} G(p)\exp(p\bar{t})\,(p - \varphi)$ (A7)

496   where φ is the location of the pole of $G(p)$ in Eq. (A1). The function $G(p)$ has infinite

497   simple poles at the negative part of the real axis in the complex plane. The locations of these

498   poles are the roots of equation that

499     $p(p\varepsilon\kappa_z \cosh\lambda + \kappa_z\lambda\sinh\lambda) = 0$ (A8)

500   which is obtained by letting the denominator in Eq. (A1) to be zero. Obviously, one pole is at

501     $p = 0$, and its residue based on Eqs. (A1) and (A7) with $\lambda_{m,n} = \sqrt{f_{m,n}/\kappa_z}$ can be expressed

502   as

503     $\phi_{m,n} = \cosh[(1 + \bar{z})\lambda_{m,n}]/(\kappa_z\lambda_{m,n}\sinh\lambda_{m,n})$ (A9)

504   The locations of other poles of $G(p)$ are the roots of the equation that

505     $p\varepsilon\kappa_z \cosh\lambda + \kappa_z\lambda\sinh\lambda = 0$ (A10)

506   which is the expression in the parentheses in Eq. (A8). One pole is between $p = 0$ and $p = -f_{m,n}$.

507   Let $\lambda = \lambda_{0,m,n}$, and Eq. (A2) becomes $p = -f_{m,n} + \kappa_z\lambda_{0,m,n}^2$. Substituting $\lambda = \lambda_{0,m,n}$, $p =$

508     $-f_{m,n} + \kappa_z\lambda_{0,m,n}^2$, $\cosh\lambda_{0,m,n} = [\exp\lambda_{0,m,n} + \exp(-\lambda_{0,m,n})]/2$ and $\sinh\lambda_{0,m,n} =$

509     $[\exp\lambda_{0,m,n} - \exp(-\lambda_{0,m,n})]/2$ into Eq. (A9) and rearranging the result lead to Eq. (32). The

510   pole is at $p = -f_{m,n} + \kappa_z\lambda_{0,m,n}^2$ with a numerical value of $\lambda_{0,m,n}$. With Eq. (A1), Eq. (A7)

511   equals

512     $Res = \lim\limits_{p\to\varphi} \dfrac{\cosh[(1+\bar{z})\lambda]}{p(p\varepsilon\kappa_z\cosh\lambda + \kappa_z\lambda\sinh\lambda)}\exp(p\bar{t})(p - \varphi)$ (A11)

513   Apply L'Hospital's Rule to Eq. (A11), and then we have

514     $Res = \lim\limits_{p\to\varphi} \dfrac{-2\lambda\cosh[(1+\bar{z})\lambda]}{p[(1+2\varepsilon\kappa_z)\lambda\cosh\lambda + (1-\varepsilon p)\sinh\lambda]}\exp(p\bar{t})$ (A12)

515   The residue for the pole at $p = -f_{m,n} + \kappa_z\lambda_{0,m,n}^2$ can be defined as

516     $\phi_{0,m,n} = \dfrac{-2\lambda_{0,m,n}\cosh[(1+\bar{z})\lambda_{0,m,n}]\exp(-\gamma_{0,m,n}\bar{t})}{\gamma_{0,m,n}[(1+2\varepsilon\kappa_z)\lambda_{0,m,n}\cosh\lambda_{0,m,n} + (1-\varepsilon\gamma_{0,m,n})\sinh\lambda_{0,m,n}]}$ (A13)

517   which is obtained by Eq. (A12) with $\lambda = \lambda_{0,m,n}$ and $p = -f_{m,n} + \kappa_z\lambda_{0,m,n}^2 = \gamma_{0,m,n}$. On the

518   other hand, infinite poles behind $p = -f_{m,n}$ are at $p = \gamma_{j,m,n}$ where $j \in 1, 2, 3, \dots \infty$. Let $\lambda =$

519     $\sqrt{-1}\lambda_{j,m,n}$, and Eq. (A2) yields $p = -f_{m,n} - \kappa_z\lambda_{j,m,n}^2$. Substituting $\lambda = \sqrt{-1}\lambda_{j,m,n}$, $p =$

520     $-f_{m,n} - \kappa_z\lambda_{j,m,n}^2$, $\cosh(\sqrt{-1}\lambda_{j,m,n}) = \cos\lambda_{j,m,n}$, and $\sinh(\sqrt{-1}\lambda_{j,m,n}) = \sqrt{-1}\sin\lambda_{j,m,n}$

521   into Eq. (A9) and rearranging the result gives rise to Eq. (31). These poles are at $p = -f_{m,n} -$

522 $\kappa_z \lambda_{j,m,n}^2$ with numerical values of $\lambda_{j,m,n}$. On the basis of Eq. (A12) with $\lambda = \sqrt{-1}\lambda_{j,m,n}$ and

523 $p = -f_{m,n} - \kappa_z \lambda_{j,m,n}^2 = \gamma_{j,m,n}$, the residues for these poles at $p = -f_{m,n} - \kappa_z \lambda_{j,m,n}^2$ can be

524 expressed as

525 $$\phi_{j,m,n} = \frac{-2\lambda_{j,m,n}\cos[(1+\bar{z})\lambda_{j,m,n}]\exp(-\gamma_{j,m,n}\bar{t})}{\gamma_{j,m,n}[(1+2\varepsilon\kappa_z)\lambda_{j,m,n}\cos\lambda_{j,m,n}+(1-\varepsilon\gamma_{j,m,n})\sin\lambda_{j,m,n}]} \tag{A14}$$

526 As a result, the inverse Laplace transform for Eq. (A1) is the sum of Eqs. (A9) and (A13) and

527 a simple series expended in the RHS function in Eq. (A14) (i.e., $\phi_{m,n} + \phi_{0,m,n} + \sum_{j=1}^{\infty} \phi_{j,m,n}$).

528 Finally, Eq. (30) can be derived after taking the inverse double-integral transform for the result

529 using the formula that (Latinopoulos, 1985, Eq. (14))

530 $$\bar{h}(\bar{x}, \bar{y}, \bar{z}, \bar{t}) = \xi \sum_{m=1}^{\infty} \sum_{n=1}^{\infty} (\phi_{m,n} + \phi_{0,m,n} + \sum_{j=1}^{\infty} \phi_{j,m,n})F_m F_n U_m U_n \tag{A15}$$

531 where ξ and $U_m U_n$ result from $\xi U_m U_n$ in Eq. (28).

532

539

540 **References**

541 Bansal, R. K., and Das, S. K.: Analytical Study of Water Table Fluctuation in Unconfined

542   Aquifers due to Varying Bed Slopes and Spatial Location of the Recharge Basin, J Hydrol

543   Eng, 15, 909-917, 2010.

544 Bansal, R. K., and Teloglou, I. S.: An Analytical Study of Groundwater Fluctuations in

545   Unconfined Leaky Aquifers Induced by Multiple Localized Recharge and Withdrawal,

546   Global Nest J, 15, 394-407, 2013.

547   Bear, J.: Hydraulics of Groundwater, McGraw-Hill, New York, 158, 1979.

548   Bruggeman, G. A.: Analytical Solutions of Geohydrological Problems, Elsevier, Netherlands,

549   326, 1999.

550   Chang, Y. C., and Yeh, H. D.: Analytical solution for groundwater flow in an anisotropic

551   sloping aquifer with arbitrarily located multiwells, J Hydrol, 347, 143-152, 2007.

552   Chor, T. L., and Dias, N. L.: Technical Note: A simple generalization of the Brutsaert and

553   Nieber analysis, Hydrol Earth Syst Sc, 19, 2755-2761, 2015.

554   Dagan, G.: Linearized solutions of free surface groundwater flow with uniform recharge, J

555   Geophys. Res., 72, 1183-1193, 1967.

556   Hansen, B. P., and Lapham, W. W.: Geohydrology and simulated ground-water flow,

557   Plymouth-Carver Aquifer, southeastern Massachusetts, US Geological Survey, USA,

558   Report 90-4204, 1992.

559   Hantush, M. S.: Growth of a ground water ridge in response to deep percolation, Symposium

560   on Transient Ground water Hydraulics, Ft. Collins, Colorado, 25-27 July, 1963.

561   Hantush, M. S.: Growth and decay of groundwater-mounds in response to uniform percolation,

562   Water Resour Res, 3, 227-234, 10.1029/WR003i001p00227, 1967.

563   Hsieh, P. C., Hsu, H. T., Liao, C. B., and Chiueh, P. T.: Groundwater response to tidal

564   fluctuation and rainfall in a coastal aquifer, J Hydrol, 521, 132-140, 2015.

565   Illas, T. S., Thomas, Z. S., and Andreas, P. C.: Water table fluctuation in aquifers overlying a

566   semi-impervious layer due to transient recharge from a circular basin, J Hydrol, 348, 215-

567   223, 2008.

568   Ireson, A. M., and Butler, A. P.: A critical assessment of simple recharge models: application

569   to the UK Chalk, Hydrol Earth Syst Sc, 17, 2083-2096, 2013.

570   Latinopoulos, P.: Analytical Solutions for Periodic Well Recharge in Rectangular Aquifers

571   with 3rd-Kind Boundary-Conditions, J Hydrol, 77, 293-306, 1985.

572   Latinopoulos, P.: Analytical Solutions for Strip Basin Recharge to Aquifers with Cauchy

573   Boundary-Conditions, J Hydrol, 83, 197-206, 1986.

574   Liang, X. Y., and Zhang, Y. K.: Analyses of uncertainties and scaling of groundwater level

575   fluctuations, Hydrol Earth Syst Sc, 19, 2971-2979, 2015.

576   Liang, X. Y., Zhang, Y. K., and Schilling, K. E.: Analytical solutions for two-dimensional

577   groundwater flow with subsurface drainage tiles, J Hydrol, 521, 556-564, 2015.

578   Manglik, A., Rai, S. N., and Singh, R. N.: Response of an Unconfined Aquifer Induced by

579   Time Varying Recharge from a Rectangular Basin, Water Resour Manag, 11, 185-196,

580   1997.

581   Manglik, A., and Rai, S. N.: Two-Dimensional Modelling of Water Table Fluctuations due to

582   Time-Varying Recharge from Rectangular Basin, Water Resour Manag, 12, 467-475,

583   1998.

584   Marino, M. A.: Hele-Shaw model study of the growth and decay of groundwater ridges, Journal

585   of Geophysical Research, 72, 1195-1205, 10.1029/JZ072i004p01195, 1967.

586   Neuman, S. P.: Effect of partial penetration on flow in unconfined aquifers considering delayed

587   gravity response, Water Resour Res, 10, 303-312, 10.1029/WR010i002p00303, 1974.

588   Ostendorf, D. W., DeGroot, D. J., and Hinlein, E. S.: Unconfined aquifer response to

589   infiltration basins and shallow pump tests, J Hydrol, 338, 132-144, 2007.

590   Rai, S. N., Ramana, D. V., and Singh, R. N.: On the Prediction of Ground-Water Mound

591   Formation in Response to Transient Recharge from a Circular Basin, Water Resour Manag,

592   12, 271-284, 1998.

593   Rai, S. N., Manglik, A., and Singh, V. S.: Water table fluctuation owing to time-varying

594   recharge, pumping and leakage, J Hydrol, 324, 350-358, 2006.

595   Ramana, D. V., Rai, S. N., and Singh, R. N.: Water table fluctuation due to transient recharge

596   in a 2-D aquifer system with inclined base, Water Resour Manag, 9, 127-138,

597   10.1007/BF00872464, 1995.

598   Rao, N. H., and Sarma, P. B. S.: Growth of Groundwater Mound in Response to Recharge,

599   Ground Water, 18, 587-595, 1980.

600   Rao, N. H., and Sarma, P. B. S.: Recharge to Aquifers with Mixed Boundaries, J Hydrol, 74,

601   43-51, 1984.

602   Schmitz, G., and Edenhofer, J.: Semi Analytical Solution for the Groundwater Mound Problem,

603   Adv Water Resour, 11, 21-24, 1988.

604   Singh, R.: Prediction of mound geometry under recharge basins, Water Resour Res, 12, 775-

605   780, 10.1029/WR012i004p00775, 1976.

606   Singh, S. K.: Rate and volume of stream flow depletion due to unsteady pumping, J Irrig Drain

607   E-Asce, 131, 539-545, 2005.

608   Tartakovsky, G. D., and Neuman, S. P.: Three-dimensional saturated-unsaturated flow with

609   axial symmetry to a partially penetrating well in a compressible unconfined aquifer, Water

610   Resour Res, 43, 2007.

611   van der Spek, J. E., Bogaard, T. A., and Bakker, M.: Characterization of groundwater dynamics

612   in landslides in varved clays, Hydrol Earth Syst Sc, 17, 2171-2183, 2013.

613   Wang, C. T., and Yeh, H. D.: Obtaining the steady-state drawdown solutions of constant-head

614   and constant-flux tests, Hydrol Process, 22, 3456-3461, 2008.

615   Yeh, H. D., Chang, Y. C., and Zlotnik, V. A.: Stream depletion rate and volume from

616   groundwater pumping in wedge-shape aquifers, J Hydrol, 349, 501-511, 2008.

617   Yeh, H. D., and Chang, Y. C.: Recent advances in modeling of well hydraulics, Adv Water

618   Resour, 51, 27-51, 2013.

619   Zlotnik, V., and Ledder, G.: Groundwater-Flow in a Compressible Unconfined Aquifer with

620   Uniform Circular Recharge, Water Resour Res, 28, 1619-1630, 1992.

621   Zlotnik, V., and Ledder, G.: Groundwater Velocity in an Unconfined Aquifer with Rectangular

622   Areal Recharge, Water Resour Res, 29, 2827-2834, 1993.

623

1   **Table 1.** Classification of existing analytical solutions involving localized recharge.

References	Aquifer domain	Aquifer boundary conditions	Recharge Region	Rate	Remarks
1D groundwater flow					
Hantush (1963)	Infinite extent	None	Strip	Constant	
Rao and Sarma (1980)	Finite extent	Dirichlet	Strip	Constant	
Rao and Sarma (1984)	Finite extent	Dirichlet and no-flow	Strip	Constant	
Latinopoulos (1986)	Finite extent	Robin and Dirichlet/no-flow	Strip	Seasonal pulse	
Bansal and Das (2010)	Semi-infinite extent	Dirichlet	Strip	Constant	Sloping aquifer bottom
2D groundwater flow					
Hantush (1967)	Infinite extent	None	Rectangle	Constant	
Manglik et al. (1997)	Rectangle	No-flow	Rectangle	Arbitrary function of time	
Manglik and Rai (1998)	Rectangle	Dirichlet	Rectangle	Arbitrary function of time	
Bruggeman (1999)	Vertical strip	Robin	Strip	Constant	Laplace equation
Chang and Yeh (2007)	Rectangle	Dirichlet	Rectangle	Exponential decay	Sloping aquifer bottom
Bansal and Teloglou (2013)	Rectangle	Dirichlet at two adjacent sides and no-flow at the others	Rectangle	Exponential decay	Multiple recharges and pumping wells
3D groundwater flow					
Dagan (1967)	Infinite extent	None	Rectangle	Constant	Laplace equation; approximate solution
Zlotnik and Ledder (1993)	Infinite extent	None	Rectangle	Constant	Laplace equation
Radial groundwater flow					
Zlotnik and Ledder (1992)	Infinite extent with finite thickness	None	Circle	Constant	First-order free surface equation
Rai et al. (1998)	Circle	Dirichlet	Circle	Exponential decay	
Ostendorf et al. (2007)	Infinite extent with finite thickness	None	Circle	Exponential decay	First-order free surface equation
Illas et al. (2008)	Circle	Dirichlet	Circle	Exponential decay	Leaky aquifer

2

1   **Table 2.** Default values of variables and hydraulic parameters used in the text.

| Notation	Default value (unit)	Definition
h	None	Hydraulic head
(x, y, z)	None	Variables of Cartesian coordinate
t	None	Time
(K_x, K_y, K_z)	(10 m/d, 10 m/d, 1 m/d)	Aquifer hydraulic conductivities in x, y, and z directions, respectively
(S_s, S_y)	(10^{-5} m^{-1}, 0.1)	Specific storage and specific yield, respectively
I	0.1 m/d	Constant recharge rate
I_t	None	Transient recharge rate defined as $I_t(t) = I_1 + I_0 \exp(-rt)$
$(I_1 + I_0, I_1)$	(0.1 m/d, 0.05 m/d)	Initial and ultimate transient recharge rates, respectively
r	10^3 d^{-1}	Decay constant of transient recharge rate
(B, l, w)	(20 m, 1 km, 1 km)	Aquifer initial thickness and widths in x and y directions, respectively
d	50 m	Shortest distance between the edge of recharge region and an observation point
(x_1, y_1)	450 m	Location of bottom left corner of recharge region
(a, b)	100 m	Widths of recharge region in x and y directions, respectively
(K_1, K_2, K_3, K_4)	0.1 m/d	Hydraulic conductivities of media between aquifer and lateral boundaries 1, 2, 3 and 4, respectively
(b_1, b_2, b_3, b_4)	1 m	Widths of media between aquifer and lateral boundaries 1, 2, 3 and 4, respectively
(d_1, d_2, d_3, d_4)	450 m	Shortest distances from the edge of the region to lateral boundaries 1, 2, 3 and 4, respectively
R	None	$\min(d_1, d_2, d_3, d_4)$
$\bar{h}$	None	h/B
$\bar{R}$	None	R/d
$(\bar{x}, \bar{y}, \bar{z})$	(12, 10, −0.5)	$(x/d, y/d, z/B)$

$\bar{t}$	None	$K_x t/(S_s d^2)$
$(\kappa_y,\ \kappa_z,\ \varepsilon)$	(1, 0.625, 500)	$(K_y/K_x,\ K_z d^2/(K_x B^2),\ S_y/(S_s B))$
ξ	0.1	I/K_z
ξ_t	None	$\xi_1 + \xi_0 \exp(-\gamma \bar{t})$
$(\xi_1,\ \xi_0,\ \gamma)$	(0.05, 0.05, 2.5)	$(I_1/K_z,\ I_0/K_z,\ r S_s d^2/K_x)$
$(\bar{l},\ \bar{w},\ \bar{a},\ \bar{b})$	(20, 20, 2, 2)	$(l/d,\ w/d,\ a/d,\ b/d)$
$(\bar{x}_1,\ \bar{y}_1)$	9	$(x_1/d,\ y_1/d)$
$(\kappa_1,\ \kappa_2,\ \kappa_3,\ \kappa_4)$	0.5	$(K_1 d/(K_x b_1),\ K_2 d/(K_x b_2),\ K_3 d/(K_y b_3),\ K_4 d/(K_y b_4))$
$(\bar{d}_1,\ \bar{d}_2,\ \bar{d}_3,\ \bar{d}_4)$	9	$(d_1/d,\ d_2/d,\ d_3/d,\ d_4/d)$

1
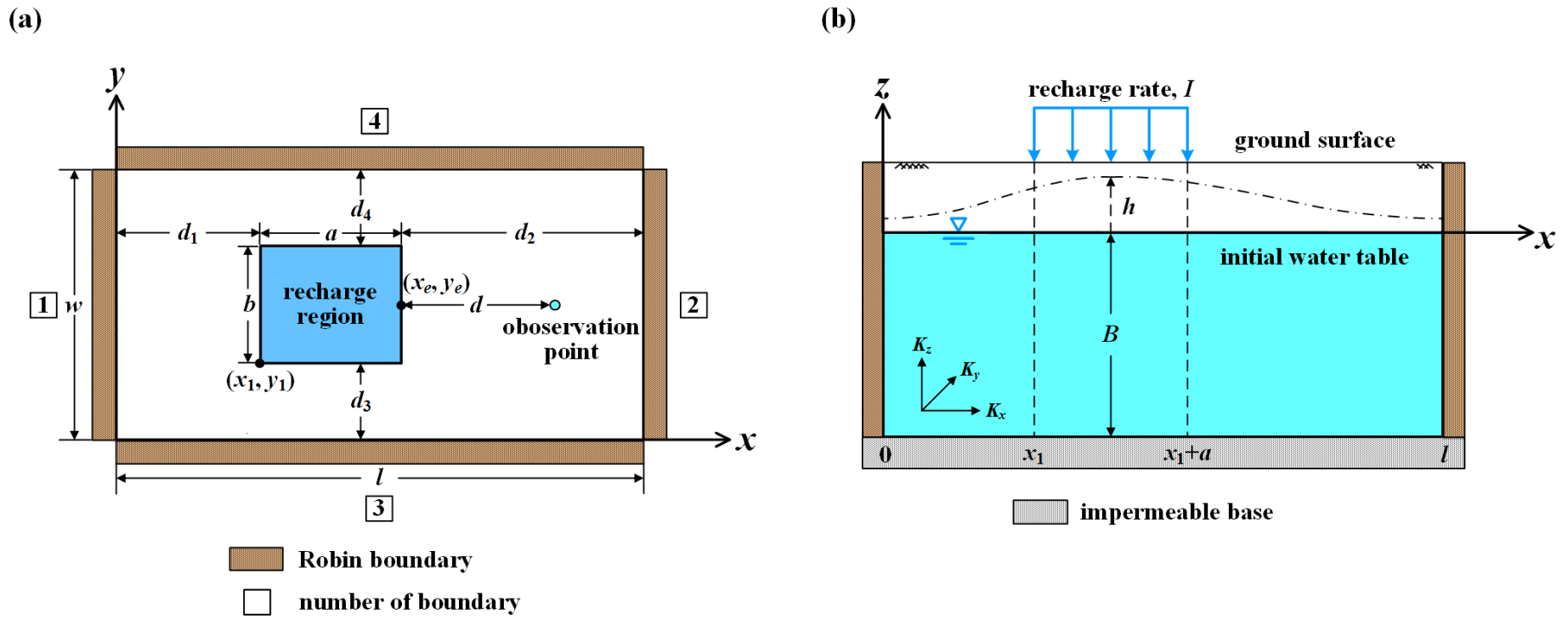
Figure 1. Schematic diagram of a rectangular-shaped unconfined aquifer with localized recharge (a) top view (b) cross section view.

1
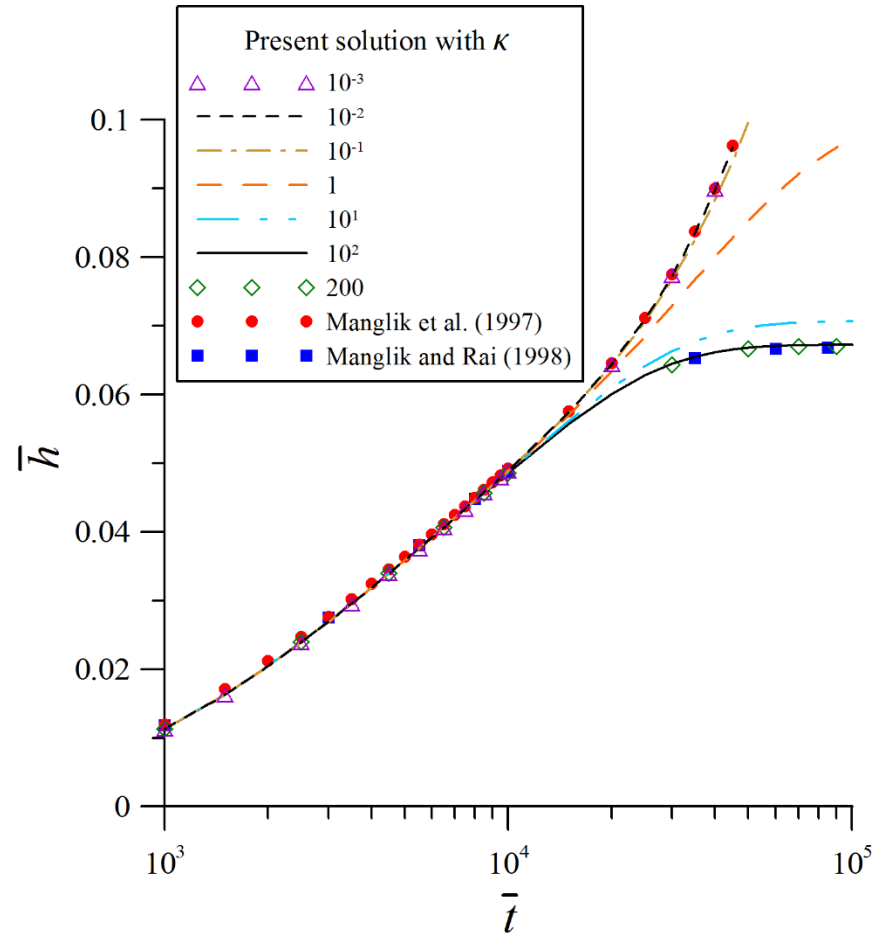
Figure 2. Temporal distributions of the dimensionless head predicted by Manglik et al. (1997) solution for a no-flow boundary, Manglik and Rai

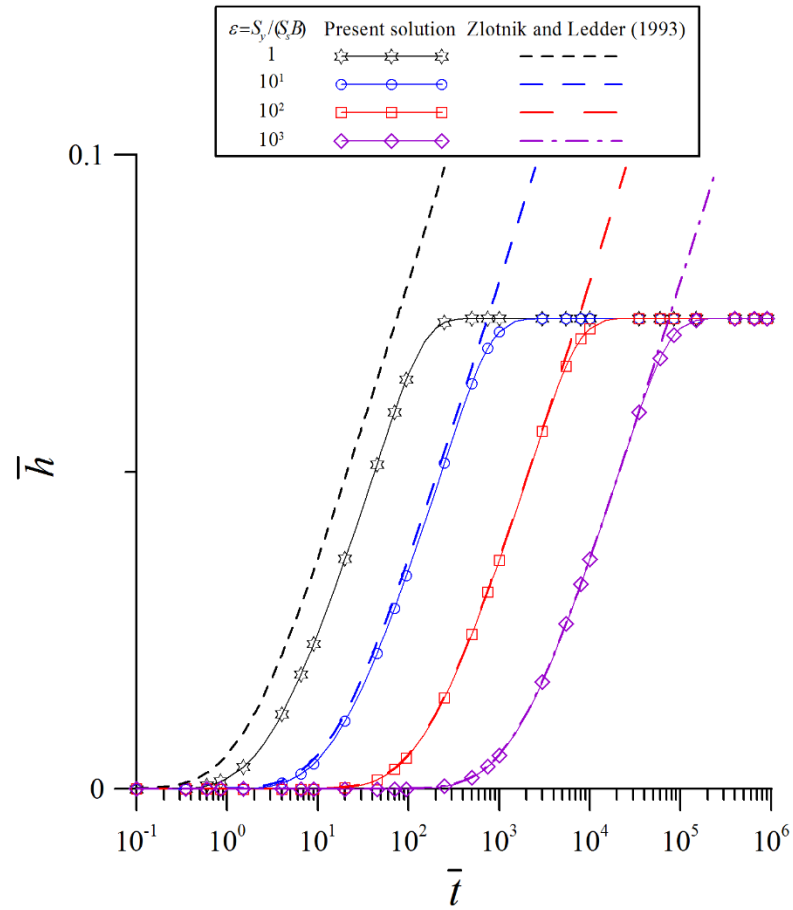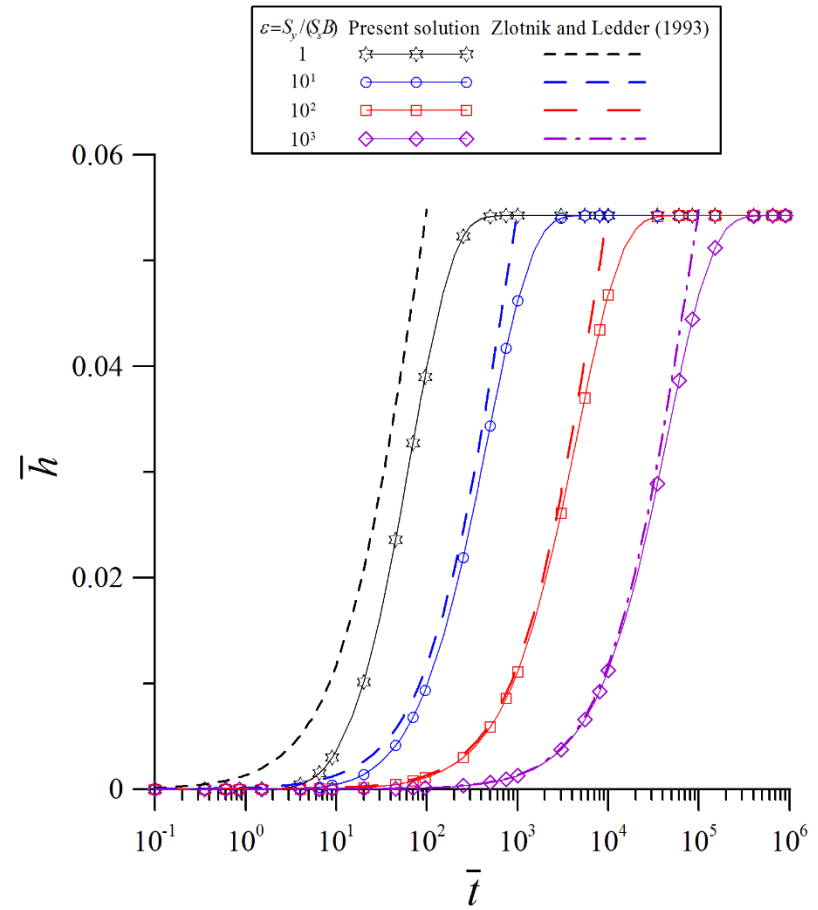(1998) solution for a Dirichlet boundary, and the present solution with $\kappa_z = 1$ for a Robin boundary.
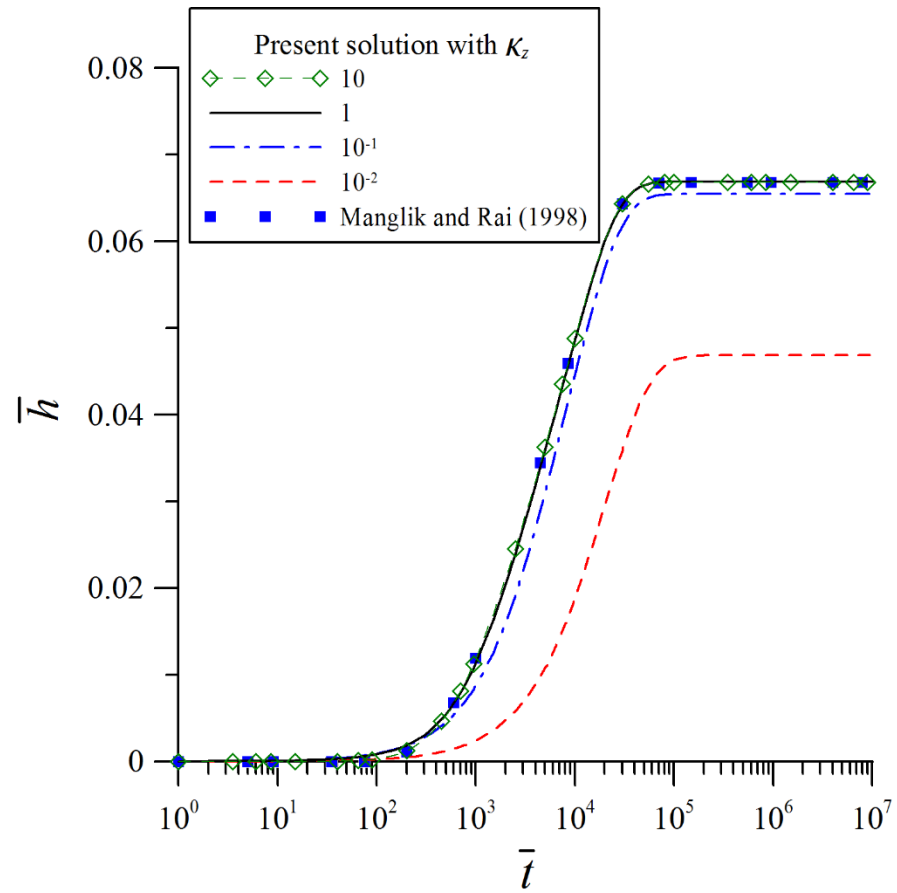
1

2　**Figure 3.** Temporal distributions of the dimensionless head predicted by Manglik and Rai (1998) solution based on 2D flow and the present
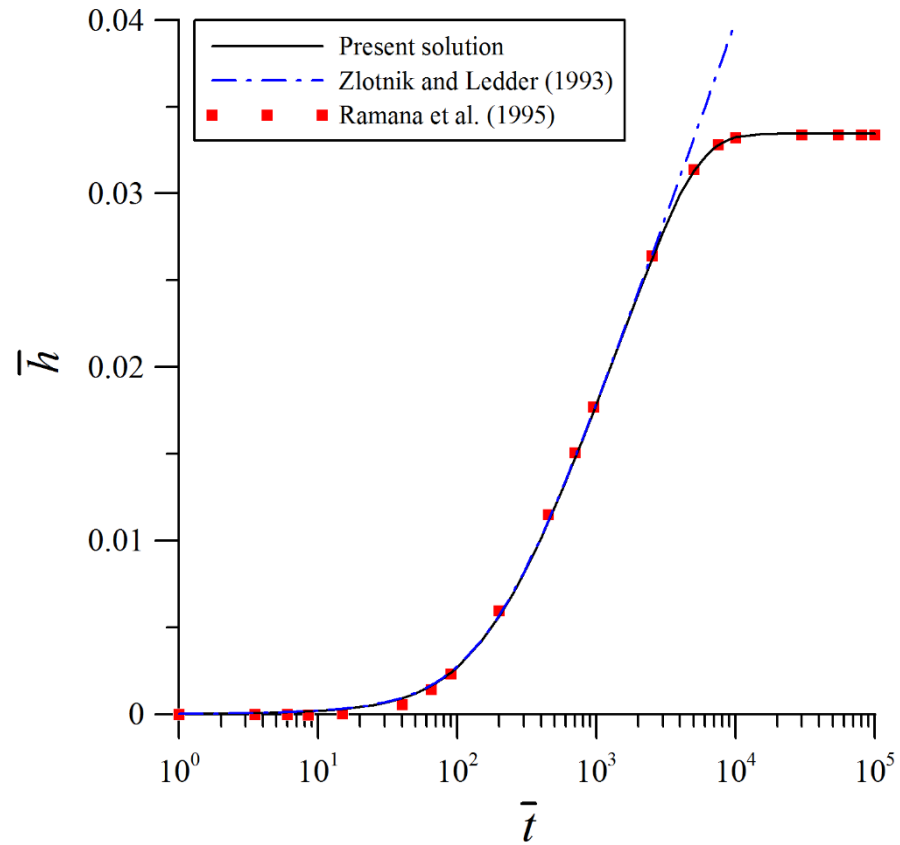
3　solution for 3D flow with various κ_z.

4

Figure 4. Temporal distributions of the dimensionless head for (a) $\kappa_z = 10^{-2}$ and (b) $\kappa_z = 10$ predicted by Zlotnik and Ledder (1993) solution based on the assumption of $S_s = 0$ and the present solution relaxing the assumption.

1

Figure 5. Temporal distributions of the dimensionless head subject to a transient recharge rate predicted by Ramana et al. (1995) solution, Zlotnik

and Ledder (1993) solution, and the present solution with $\kappa_z = 1$, $\kappa = 100$, and $\varepsilon = 100$.
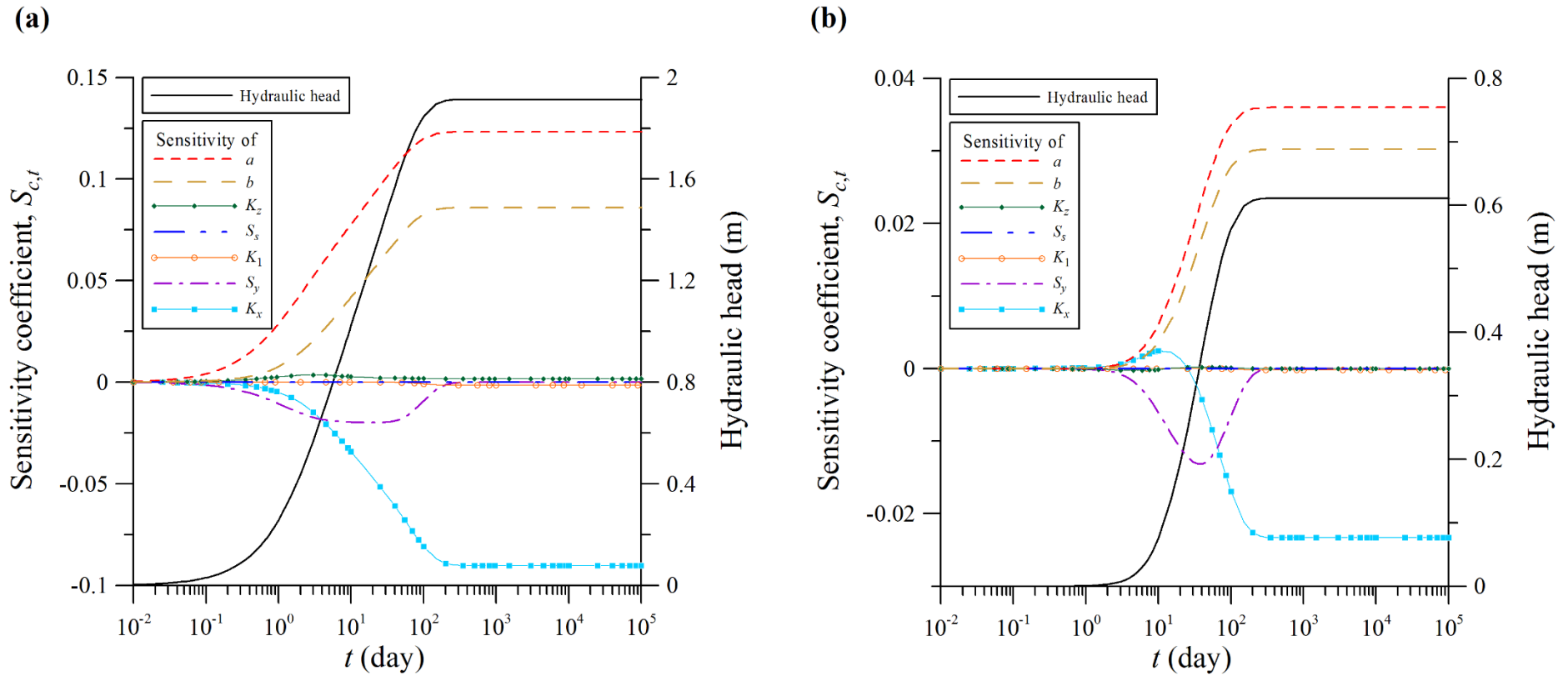
Figure 6. Temporal distributions of the normalized sensitivity coefficients of the hydraulic head at the observation points of (a) $(x, y, z) = (555, 500, -10)$ and (b) $(x, y, z) = (800, 500, -10)$ to the changes in parameters a, b, K_z, S_s, K_1, S_y, and K_x.